International Journal of Thermal Sciences 49 (2010) 1138–1146

Contents lists available at ScienceDirect

International Journal of Thermal Sciences

journal homepage: www.elsevier.com/locate/ijts

Investigation for the dual phase lag behavior of bio-heat transfer

Kuo-Chi Liu [a,*], Han-Taw Chen [b]

[a] Department of Mechanical Engineering, Far East University, 49 Chung Hua Rd., Hsin-Shih, Tainan 744, Taiwan
[b] Department of Mechanical Engineering, National Cheng Kung University, Tainan 701, Taiwan

ARTICLE INFO

Article history:
Received 22 October 2009
Received in revised form
28 January 2010
Accepted 15 February 2010
Available online 20 March 2010

Keywords:
Bi-layer solid sphere
Bio-heat transfer
Dual phase lag model
Inverse analysis

ABSTRACT

The success of hyperthermia treatment depends on the precise prediction and control of temperature distribution in the tissue. It was absolutely a necessity for hyperthermia treatment planning to understand the heat transport occurring in biological tissue. The tissue is highly non-homogenous, and non-Fourier thermal behavior in biological tissue has been experimentally observed. The dual phase lag model of heat conduction has been used to interpret the non-Fourier thermal behavior. This work attempts to be an extension study of Antaki [12] and explore whether the DPL thermal behavior exists in tissue. The inverse non-Fourier bio-heat transfer problem in the bi-layer spherical geometry is analyzed. In order to further address whether the dual phase lag model of bio-heat transfer merits additional study, the comparisons of the history of temperature increase among the present calculated results, the calculated values from the classical bio-heat transfer equation, and the experimental data are made for various measurement locations.

1. Introduction

It is an instinct of the human body to use heat to fight disease. The use of heat in order to necrotize undesirable tissue for therapeutic purposes has been in many applications, such as laser, microwave and magnetic fluid hyperthermia. The success of these thermal therapies depends on the precise prediction and control of temperature in the tissue. An ideal thermal treatment should selectively destroy the target region without damaging the surrounding healthy tissue. Knowledge of temperature distribution in the entire treatment region is essential for limiting the temperatures in the healthy tissue to prevent damage. However, it is not easy to accurately determine the temperature field over the entire treatment region during clinical hyperthermia treatments, because the pain tolerance of patients makes the number of invasive temperature probes limited [1]. Hence, the analysis and modeling of the underlying thermal mechanisms are important to optimize the temperature distribution in the treated region. As Wren et al. [2] stated, in order to further improve the thermal treatment methods, bio-heat models are essential during development of equipment, for pre-planning purposes, for on-line monitoring and decision support as well as for evaluation of the extent of thermal damage.

The most commonly used model among many bio-heat transfer models is the Pennes bio-heat model for simplicity and validity. The Pennes bio-heat equation was developed on the base of the classical Fourier's law that depicts an infinitely fast propagation of thermal signal. However, the contents of the literatures [3–5] indicated that thermal behavior in non-homogenous media needs a relaxation time to accumulate enough energy to transfer to the nearest element and the relaxation time in biological tissues is to be 20–30 s. The experiments of Mitra et al. [6] with processed meat showed the evidence of non-Fourier conduction in tissue. The relaxation time for processed meat is of the order of 15 s. Roetzel et al. [7] also made the experimental investigation for processed meat and had the value of relaxation time about 2 s. Obviously, the concept of infinite heat propagation velocity is incompatible with physical reality in tissues. As a result, the thermal wave model of bio-heat transfer received the attention from relevant researchers [8–11].

For developing better tools to predict transient temperature in tissue, Antaki [12] treated the processed meat as a composite material that is a heterogeneous compacted mixture of meat particles and water and used the dual phase lag (DPL) model to interpret heat conduction in it. After that, Liu and Chen [13] studied temperature rise behavior in a two-layer concentric spherical region during magnetic tumor hyperthermia treatment with the DPL model. The DPL model describes a macroscopic temperature with the micro-structural effect by introducing the phase lag times of heat flux and temperature gradient. Specifically, the DPL model combines the wave features of hyperbolic conduction with a diffusion-like feature of the evidence not captured by the hyperbolic case [12]. Recently, Zhang [14] developed a bio-heat equation,

* Corresponding author.
E-mail addresses: kuochi.liu@msa.hinet.net, kcliu@cc.feu.edu.tw (K.-C. Liu).

1290-0729/$ – see front matter © 2010 Elsevier Masson SAS. All rights reserved.
doi:10.1016/j.ijthermalsci.2010.02.007

Nomenclature

A	estimated parameter
c	specific heat of tissue, J/kg K
c_b	specific heat of blood, J/kg K
$\mathrm{d_n}$	correction of A_n
e_m	deviation between θ_m^{cal} and θ_m^{mea}
f	parameter defined in Eq. (21)
H	new dependent variable, $H = r(T - T_0)$
$\tilde{H}$	Laplace transform of H
k	thermal conductivity, W/m K
K	parameter defined in Eq. (22)
ℓ	distance between two neighboring nodes, m
M	total number of nodes
N	total number of estimated parameters
P	power density, W/m^3
q_m	metabolic heat generation, W/m^3
q_r	spatial heating source, W/m^3
r	space coordinate, m
R	radius of tumor, m
s	Laplace transform parameter
t	time, s
T	temperature of tissue, K
T_b	arterial temperature, K
T_0	initial temperature of tissue, K
w_b	perfusion rate of blood, m^3/s/m^3
ω_{mn}	parameter defined in Eq. (42)

Greek symbols

δ_{mn}	Kronecker delta
θ	temperature increase defined in Eq. (35)
ε	standard deviation of the measurements
λ	parameter defined in Eq. (20)
ρ	density, kg/m^3
ψ	volume fraction of magnetic particles
τ_q	phase lag of the heat flux, s
τ_T	phase lag of the temperature gradient, s

Superscripts

cal	calculated value
mea	measured data

Subscripts

g	magnetic particle
i	node number
j	number of sub-space domain
k	number of layer
m	number of time node
n	number of estimated parameter
t	tumor tissue

which was also called the DPL bio-heat equation, for the perfused tissue based on the nonequilibrium heat transfer between the blood in artery and the surrounding tissue. However, the tissue was regarded as solid media, not non-homogenous media, and the behavior of heat conduction in the tissue was still described with the classical Fourier's law. Although Antaki [12] predicted the phase lag time of heat flux to be 14–16 s and the phase lag time of temperature gradient to be 0.043–0.056 s for processed meat with the experimental data measured by Mitra et al. [6], more experimental results are required for showing the physical meanings of the DPL mode in heat transfer in tissue.

For the study of magnetic tumor hyperthermia, Andrä et al. [15] took a spherical region containing magnetic particles embedded in extended muscle tissue as model of small carcinoma and measured the spatial distribution of temperature as function of exposure time around the spherical composite. This work attempts to be an extension study of Antaki [12] and explore whether the DPL thermal behavior exists in tissue. The experimental data of Andrä et al. [15] would be used to estimate the phase lag times based on the DPL model. It is needed to make the inverse analysis of a DPL bio-heat transfer problem in the bi-layer spherical tissue. There are mathematical difficulties in dealing with the non-Fourier heat transfer problem. And also, the inverse problem is ill-posed because a small measurement error induces a large estimated error [17,18]. Therefore, the studies about the inverse non-Fourier heat transfer problem are not numerous. The literatures [16–20] mainly estimated the boundary conditions with the analytical solution in conjunction with measurement errors. Liu [21] had used the experimental data of the concentration history to predict the diffusion coefficient and the relaxation time during the rapid transient mass transfer of NaCl diffusing in H_2O based on the hyperbolic mass diffusion equation. The present problem needs to estimate four unknown phase lag times simultaneously. The geometry effect and the interfacial boundary conditions introduce the complexity and cause more mathematical difficulties. In order to further address whether the dual phase lag model of bio-heat transfer merits additional study, the comparisons of the temperature increase history among the present calculated results, the calculated values from the classical bio-heat transfer equation, and the experimental data are made for various measurement locations.

2. Problem description

In magnetic tumor hyperthermia, fine magnetic particles are localized at the tumor tissue. The literatures [15,22,23] regarded the small tumor as a solid sphere with the radius R and becomes a heat source of constant power density P in the small tumor for excitation of alternating magnetic field. The heat source is assumed to be surrounded by a medium of homogeneous heat conductivity. The heating material, e.g. magnetic particles injected into the tumor, and the surrounding medium are characterized by the values of their heat conductivity k, their specific heat capacity c, and their mass density ρ. Because of the spherical symmetry of the system and the homogeneous time-independent power density P inside the sphere the temperature distribution depends only on distance r from the center of the sphere and on time t.

For experimental study, Andrä et al. [15] made the heating material of carrageenan and a variable amount of magnetite with a mean grain size of 1 μm and embedded it in extended muscle tissue from cow. The composite was formed as cylinder which diameter and height are 5.5 mm. In accordance with the contents of the literatures [24], the edges of the cylinder have a stronger heat transfer into the surroundings and remain cooler, and the isotherms would approach circle at the central cross-section. Andrä et al. [15], thus, specified the measurement locations in sphere radius. Fitting in with the experimental data, this paper regards the composite as a sphere of 6.3 mm diameter as Andrä et al. [15] did. The spatial distribution of temperature increase as function of exposure time was measured with thermocouples as shown in Fig. 1.The region $0 \le r \le R$ is a composite of carrageenan and magnetic particles. The effective density ρ_1 and the effective specific heat c_1 are calculated as $\rho_1 = \psi\rho_g + (1-\psi)\rho_t$

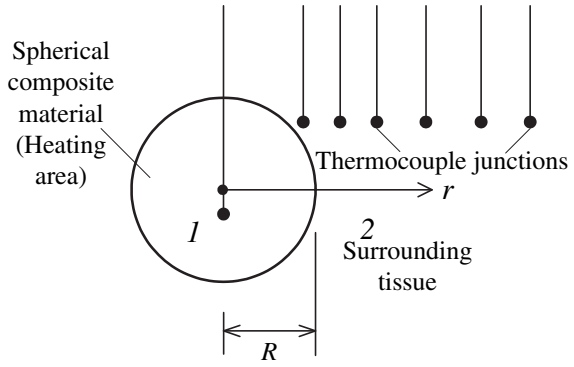

Fig. 1. Illustration for model configuration.

and $c_1 = \psi c_g + (1-\psi)c_t$, where subscripts g and t symbol the magnetic particles and the carrageenan. ψ is the volume fraction of magnetic particles inside the sphere. In accordance with Andrä et al. [15], the spatial distribution of particles of high heat conductivity in a matrix of low heat conductivity may be approximated by a serial arrangement of the two materials with the respective volume fractions

$$k_1 = \left(\frac{\psi}{k_g} + \frac{1-\psi}{k_t}\right)^{-1} \tag{1}$$

In the experiment, the composite consists of 106 mg magnetite and carrageenan gel with the following parameters: $k_1 = 0.778$ W/(K m), $\rho_1 = 1.66$ g/cm^3, $c_1 = 2.54$ J/(g K), $R = 3.15$ mm and a power density of 6.15 W/cm^3. The corresponding parameters of the surrounding muscle tissue were taken as: $k_2 = 0.642$ W/(K m), $\rho_2 = 1$ g/cm^3, $c_2 = 3.72$ J/(g K).

Tzou [25] proposed the DPL model that allows either the temperature gradient to precede heat flux vector or the heat flux vector to precede the temperature gradient. The linearized form of the DPL model is based on the equation

$$\tau_q \frac{\partial q}{\partial t} + q = -k\frac{\partial T}{\partial r} - k\tau_T \frac{\partial^2 T}{\partial t \partial r} \tag{2}$$

where T is the temperature and q is the heat flux. τ_q means the phase lag of the heat flux and τ_T means the phase lag of the temperature gradient. The heat flux precedes the temperature gradient for $\tau_q < \tau_T$. The temperature gradient precedes the heat flux for $\tau_q > \tau_T$. The DPL model depicts that not only the temperature gradient may precede the heat flux, but also the heat flux may precede the temperature gradient. The values of τ_q and τ_T may be different in tumor and normal tissue as well as the other physiological parameters. For convenience of estimation, the present work assumes τ_q and τ_T constant and predicts them from the experimental data given by Andrä et al. [15]. As $\tau_q = \tau_T = 0$, the DPL model would become the classical model of heat transfer. The classical bio-heat transfer equation was derived based on the classical model of heat transfer.

In a local energy balance, the one-dimensional energy equation of the present problem is given as

$$\rho c \frac{\partial T}{\partial t} = -\frac{\partial q}{\partial r} - \frac{2}{r}q + w_b \rho_b c_b (T_b - T) + q_m + q_r \tag{3}$$

where ρ_b and c_b respectively are the density and specific heat. The spatial heating source q_r is defined as $q_r = Pu(t)$, where $u(t)$ is a step function. The present work omits the metabolic heat generation q_m and the perfusion rate of blood w_b for that the experiment was not performed with living tissue.

Substituting Eq. (2) into the energy conservation equation (3) leads to the heat transport equations in the heating material and the extended muscle tissue with constant physiological parameters as the following:

$$k_1 \frac{1}{r^2}\frac{\partial}{\partial r}\left[r^2\left(\frac{\partial T_1}{\partial r} + \tau_{T1}\frac{\partial^2 T_1}{\partial t \partial r}\right)\right] = \left(1 + \tau_{q1}\frac{\partial}{\partial t}\right)\left[\rho_1 c_1 \frac{\partial T_1}{\partial t} - P\right] \quad \text{for } 0 \le r \le R \tag{4}$$

$$k_2 \frac{1}{r^2}\frac{\partial}{\partial r}\left[r^2\left(\frac{\partial T_2}{\partial r} + \tau_{T2}\frac{\partial^2 T_2}{\partial t \partial r}\right)\right] = \left(1 + \tau_{q2}\frac{\partial}{\partial t}\right)\rho_2 c_2 \frac{\partial T_2}{\partial t} \quad \text{for } R \le r \le \infty \tag{5}$$

The indices 1 and 2 mean the interior and exterior of the sphere $r \le R$, respectively.

The present work regards the temperature and the heat flux at the interface of two regions is continuous. In other words, the heat contact resistance at the interface between the two different media is neglected. The boundary conditions are described as

$$\frac{\partial T_1(0,t)}{\partial r} = 0 \quad \text{and} \quad T_1(0,t) \quad \text{is finite} \tag{6}$$

$$T_1(R,t) = T_2(R,t) \tag{7}$$

$$q_1(R,t) = q_2(R,t) \tag{8}$$

$$T_2(\infty, t) = T_0 \tag{9}$$

and the initial conditions are

$$T_k(r,0) = T_0, \ \frac{\partial T_k(r,0)}{\partial t} = 0 \text{ and } q_k(r,0) = 0 \quad k = 1,2 \tag{10}$$

3. Analytical methods

For convenience of analysis, a new dependent variable H is defined as

$$H = r(T - T_0) \tag{11}$$

Under the circumstances, Eqs. (4) and (5) in terms of H can be rewritten as

$$k_1\left(1 + \tau_{T1}\frac{\partial}{\partial t}\right)\frac{\partial^2 H_1}{\partial r^2} = \left(1 + \tau_{q1}\frac{\partial}{\partial t}\right)\left[\rho_1 c_1 \frac{\partial H_1}{\partial t} - \Pr\right] \quad \text{for } 0 \le r \le R \tag{12}$$

$$k_2\left(1 + \tau_{T2}\frac{\partial}{\partial t}\right)\frac{\partial^2 H_2}{\partial r^2} = \left(1 + \tau_{q2}\frac{\partial}{\partial t}\right)\rho_2 c_2 \frac{\partial H_2}{\partial t} \quad \text{for } R \le r \le \infty \tag{13}$$

The boundary conditions and the initial conditions become

$$H_1(0,t) = 0 \tag{14}$$

$$H_1(R,t) = H_2(R,t) \tag{15}$$

$$q_1(R,t) = q_2(R,t) \tag{16}$$

$$H_2(\infty, t) = 0 \tag{17}$$

and

$$H_k(r,0) = 0, \quad \frac{\partial H_k(r,0)}{\partial t} = 0, \text{ and } q_k(r,0) = 0 \quad k = 1,2 \tag{18}$$

The temperature increase θ is equal to

$$\theta = T - T_0 = H/r \tag{19}$$

The value of H/r at $r = 0$ is indeterminate and must be replaced by its limit as $r \to 0$. Thus the value of the transient temperature increase at the center is evaluated by using L'Hôspital's rule as

$$\theta(0,t) = T(0,t) - T_0 = \lim_{r\to 0}\frac{H}{r} = \frac{dH}{dr} \tag{20}$$

To solve the present problem, a hybrid scheme based on the Laplace transform, a modified discretization scheme, and the least-squares scheme is proposed. Please refer to Appendix A for the details of the present numerical scheme.

4. Results and discussion

Measured values of the increase of temperature for the parameters described above are plotted in Fig. 2 with symbols indicating the various reduced distances: $r/R = 1.10$; 1.39; 1.68; 1.98. The symbols are discrete values of measured temperature that were extracted from the continuous thermocouple record. These measured values were presented in Fig. 3 in Ref. [15] originally. Copy the figure from the PDF file and past on the panel of the software Litter Painter, then locate the cursor on the symbols; as a result, the values of θ and t for each symbol can be determined with the coordinates of the cursor on the 1024 × 768 pixels monitor. The experimental errors of both θ and t are within the extent of the used symbols [15]. For theoretical study, Andrä et al. [15] calculated the increase of temperature with exposure time t based on the classical bio-heat transfer equation for the corresponding parameters. Fig. 2 shows the calculated values from the classical bio-heat transfer equation are out of the extent range of the used symbols indicating measured values. This phenomenon implies that the classical bio-heat transfer equation can not completely describe the thermal behavior captured in the experiment. However, the present numerical results agree well with the calculated values given by Andrä et al. [15]. The accuracy of the present numerical scheme for the direct solution is tested.

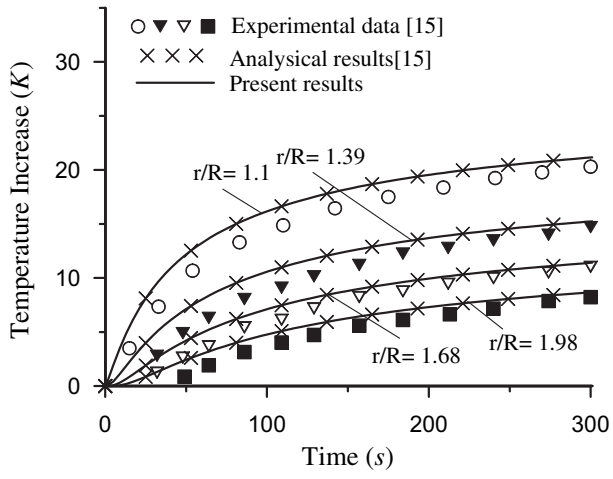

Fig. 2. Comparison of the calculated values from the classical bio-heat transfer equation with the experimental data.

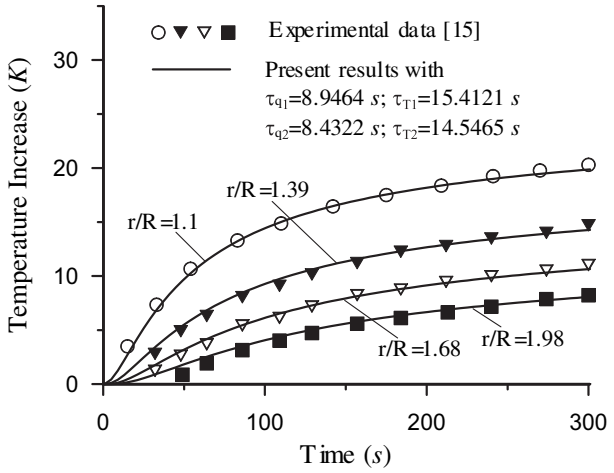

Fig. 3. Variation of temperature increase with the predicted values of τ_{q1}, τ_{T1}, τ_{q2} and τ_{T2} from the measured data at $r/R = 1.1$.

It is well known that the lag times τ_q and τ_T are the characteristic of the dual phase lag model. To explore the physical meanings of the dual phase lag model in the bio-heat transfer, evaluating the lag times τ_q and τ_T is essential work. As the previous statement, the values of τ_q and τ_T may be different in layers 1 and 2 as well as the other physiological parameters. The phase lag times, τ_{q1}, τ_{T1}, τ_{q2} and τ_{T2}, become the target estimated parameters of the present work, and the number of parameters, N, is 4. The instruments have a measurement error of 3% is common [19,20]. Therefore, in the process of inverse analysis, the standard deviation of the measurements was assumed to be a constant 0.03.The standard deviation of the measurements gets a smaller value, the estimated values of the phase lags will make the predicted temperature increase closer to the experimental data, but the inverse computation is harder to converge. In addition, there is evidence [26] that the values of the target estimated parameters in the inverse heat transfer problem should depend on location. Therefore, this work picked out four measured values from each measurement location to be one set of reference values. These four sets of reference values that have similar time nodes are presented in Table 1. Through calculations, it is found that the different reference values lead to the different estimated values of τ_{q1}, τ_{T1}, τ_{q2} and τ_{T2}, that is, the reference values affect the estimated results. This work has the predicted value of τ_q is about 7.36–8.43 s and the predicted value of τ_T is about 14.54–21.03 s for muscle tissue from cow. In Ref. [12], the value of τ_q is about 14–16 s and the value of τ_T is about 0.043–0.056 s for processed meat. The present estimated results have an obvious difference with those in Ref. [12] because the media of heat transfer are different. Comparing with the results in the literature [14], the present estimated values of τ_q and τ_T are relatively large. Antaki [12] interpreted τ_q as a delay time for contact resistance between tissue particles; τ_T was interpreted as a measure of the conduction that occurs within tissues particles. The lag time τ_q can dominate the behavior of thermal wave propagation, slow down the propagation velocity of thermal signal, and manifest the feature of thermal wave [13,27–29]. Due to the effect of τ_T, the characters of thermal wave would decay in DPL heat transfer, and heat energy would transfer at a faster rate. However, in the literature [14], the phase lags τ_q and τ_T are caused with the nonequilibrium heat transfer between the blood in artery and the surrounding tissue.

Table 1
Reference values and estimated values.

Measurement location	Reference values of θ (K) at various times $t(s)$	Estimated values of τ_{q1}, τ_{T1}, τ_{q2}, and τ_{T2} (s)
$r/R = 1.1$	$t = 83$, $\theta = 13.3$; $t = 142$, $\theta = 16.45$; $t = 209$, $\theta = 18.375$; $t = 270$, $\theta = 19.775$	$\tau_{q1} = 8.9464$, $\tau_{T1} = 15.4121$; $\tau_{q2} = 8.4322$, $\tau_{T2} = 14.5465$
$r/R = 1.39$	$t = 109$, $\theta = 9.1$; $t = 157$, $\theta = 11.2$; $t = 212$, $\theta = 12.775$; $t = 274$, $\theta = 14$	$\tau_{q1} = 7.6140$, $\tau_{T1} = 20.1088$; $\tau_{q2} = 7.3629$, $\tau_{T2} = 18.7825$
$r/R = 1.68$	$t = 109$, $\theta = 6.125$; $t = 157$, $\theta = 8.225$; $t = 212$, $\theta = 9.45$; $t = 274$, $\theta = 10.5$	$\tau_{q1} = 8.2116$, $\tau_{T1} = 21.3856$; $\tau_{q2} = 8.0080$, $\tau_{T2} = 20.5054$
$r/R = 1.98$	$t = 109$, $\theta = 4.025$; $t = 157$, $\theta = 5.6$; $t = 212$, $\theta = 6.65$; $t = 274$, $\theta = 7.875$	$\tau_{q1} = 8.1768$, $\tau_{T1} = 22.5628$; $\tau_{q2} = 7.7672$, $\tau_{T2} = 21.3071$

On the other hand, the present results were estimated with the linearized form of the DPL model. Because it is the most commonly used form to analysis the non-Fourier heat transfer problems. The literatures [3–7,12,14] estimated the values of phase lag times always base on the linearized form of the DPL or CV model. If this paper estimates the values of phase lag times with a higher order Taylor series expansion form of the DPL model, the estimated values of phase lag times may become small. Another possibility is that the present estimated values of τ_q and τ_T are affected with the structure of the composite.

To show the rationality of the estimated results, the estimated values of τ_{q1}, τ_{T1}, τ_{q2} and τ_{T2}, as shown in Table 1, were used to calculate the increase of temperature with exposure time t at the various reduced distances: $r/R = 1.10$; 1.39; 1.68; 1.98. These calculated results are plotted in Fig. 3 and Figs. B1–B3 (in Appendix B), respectively. These figures present the variation of temperature increase θ for various sets of τ_T and τ_q at various reduced distances: $r/R = 1.10$; 1.39; 1.68; 1.98. The calculated results of thermal response agree with the experimental data implies that the estimated results approximate reality and shows the efficiency of the present method for such a problem. In other words, these experimental data seem to evidence the DPL behavior in bio-heat transfer. In the mean time, the longer the distance of the measurement location from the center is, the later the beginning of thermal response is. It is the behavior of finite propagation of thermal signal. The variation curves of temperature increase θ are smooth, not like in Refs. [6,12], because the ratio of τ_T to τ_q is greater than 1. The effect of τ_T stretches out the thermal wave and destroys the sharp wave front. The results shown in Refs. [27–29] indicate that the phase lag time τ_q can dominate the speed of thermal wave propagation, but the phase lag time τ_T does not. It is also found in a detailed observation that the larger value of τ_q makes the beginning of thermal response later. As stated in Ref. [26], depending on the location of the sensor, the solution of the inverse problem may become sensible to measurement errors of the input data. The above phenomena point out that the DPL behavior of bio-heat transfer exists in tissue very possibly. The further study about the meanings of the DPL model in bio-heat transfer is worthy to do.

The comparison among the calculated results of transient temperature increase for the four sets of the predicted values of τ_{q1}, τ_{T1}, τ_{q2} and τ_{T2} at $r/R = 1.10$ and 1.39 is made, as shown in Fig. 4. There is a slight difference among them for the different predicted values of τ_{q1}, τ_{T1}, τ_{q2} and τ_{T2}. The curves are quite close because the calculated results are in the rational range of measurement errors. The comparison for $r/R = 1.68$ and 1.98 is also made. As shown in Fig. 5, the variation curves of temperature increase at $r/R = 1.68$ and 1.98 almost coincide. Essentially, the non-Fourier effect is more obvious in small-scales and small times. The temperature variation nearby the heating source would be sensible to the values of τ_q and τ_T. In the present work, $r/R = 1.10$ is the measurement location nearest the heating source. Therefore, there is a more obvious difference among the curves for $r/R = 1.10$. The calculated results present one another feature of the non-Fourier thermal behavior of bio-heat transfer.

Fig. 6 displays the comparison among the experimental data, the calculated values from the classical bio-heat transfer equation, and the present results with $\tau_{q1} = 8.9464$ s, $\tau_{T1} = 15.4121$ s, $\tau_{q2} = 8.4322$ s, and $\tau_{T2} = 14.5465$ s. It is obvious that the present results approach the

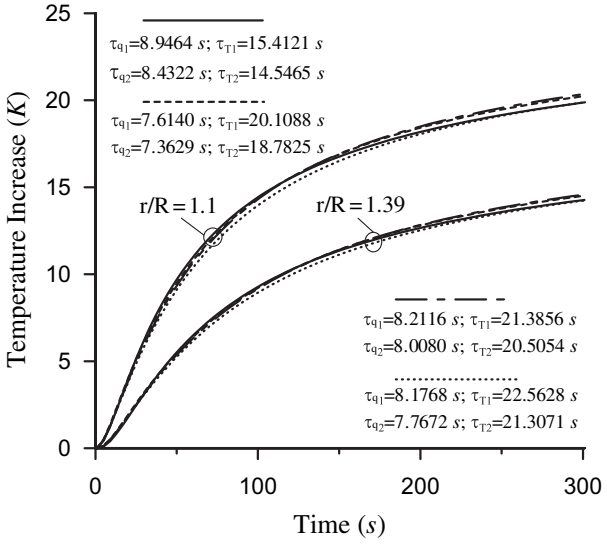

Fig. 4. Comparison among the calculated results of transient temperature increase for the four sets of predicted values of τ_{q1}, τ_{T1}, τ_{q2} and τ_{T2} at $r/R = 1.10$ and 1.39.

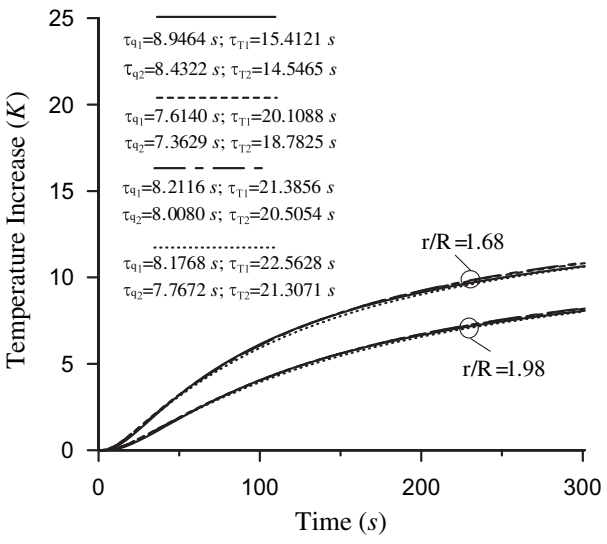

Fig. 5. Comparison among the calculated results of transient temperature increase for the four sets of predicted values of τ_{q1}, τ_{T1}, τ_{q2} and τ_{T2} at $r/R = 1.68$ and 1.98.

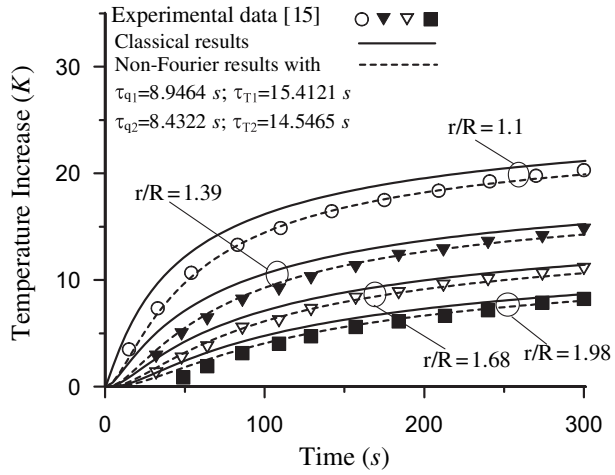

Fig. 6. Comparison among the experimental data, the calculated values from the classical bio-heat transfer equation, and the present results with $\tau_{q1} = 8.9464$ *s*, $\tau_{T1} = 15.4121$ *s*, $\tau_{q2} = 8.4322$ *s*, and $\tau_{T2} = 14.5465$ *s*.

experimental data more, even in the early times. With time passing over, the calculated values from the classical bio-heat transfer equation gradually approach the experimental data. This agrees with that the non-Fourier effect would dissipate with time. Correspondingly, the classical thermal behavior would be dominant with the distance from the center of sphere. It is observed from the results in Fig. 6 that the calculated values from the classical bio-heat transfer equation approach the experimental data with the value of r/R increasing. In other words, the thermal wave propagation is gradually replaced by the diffusion behavior with the penetration distance of thermal signal increasing. The above results enhance the features of the non-Fourier thermal behavior in the experimental data.

The predicted values, $\tau_{q1} = 8.9464$ *s*, $\tau_{T1} = 15.4121$ *s*; $\tau_{q2} = 8.4322$ *s*, $\tau_{T2} = 14.5465$ *s*, were used to calculate the temperature distributions at various times. The calculated results are presented in Fig. 7. The phase lag of the heat flux τ_q enhances the wave-like feature while the phase lag of the temperature gradient τ_T depicts the diffusion-like feature. In this case, the phase lag of the temperature gradient τ_T is greater than the phase lag of the heat flux τ_q. The diffusion-like

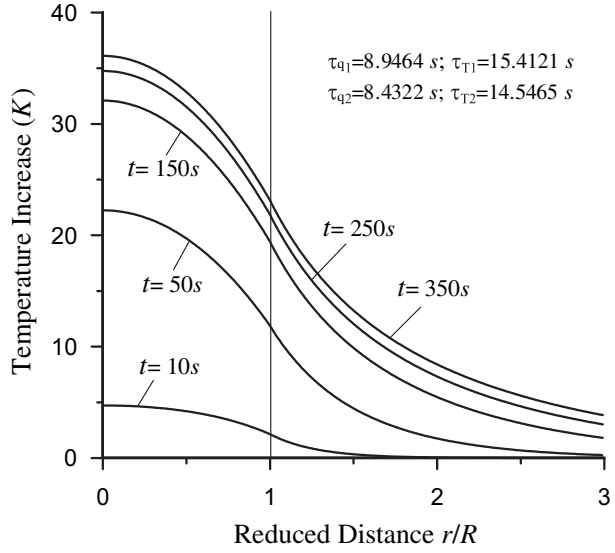

Fig. 7. Temperature distributions with $\tau_{q1} = 8.9464$ *s*, $\tau_{T1} = 15.4121$ *s*; $\tau_{q2} = 8.4322$ *s*, $\tau_{T2} = 14.5465$ *s* at various times.

feature is over the wave-like feature. The domain $0 \le r/R \le 1$ is the heating area, so the temperatures are higher. With time, heat energy gradually transfers into the surrounding medium and make the temperatures increase, then the temperature distribution in the heating area approach a steady situation. Though the location $r = 0$ is a singular point in this problem, the present numerical results are stable and have the finite value. It presents that the present numerical scheme is stable for analyzing such problems.

5. Conclusions

This work investigates the dual phase lag thermal behavior in tissue through an inverse bio-heat transfer problem in the spherical coordinate system. The values of the phase lag times, τ_q and τ_T, are estimated in accordance with the experiment data. The calculated results of the history of temperature increase agree with the experimental data at various measurement locations. Various features of the non-Fourier thermal behavior are observed from the present results. The beginning of thermal response is later with the longer distance of the measurement location from the center. It is the behavior of finite propagation of thermal signal. The larger value of τ_q makes the beginning of thermal response later. The present results gradually close to the calculated values from the classical bio-heat transfer equation with time. This phenomenon agrees with that the non-Fourier effect would dissipate with time. In the mean time, the classical thermal behavior would be dominant with the distance from the center of sphere. These features give the first evidence to the dual phase lag thermal behavior in muscle tissue from cow.

There exists a lot of controversies in the literature about whether or not DPL conduction and, more generally, any non-Fourier conduction is important for biological tissues, as stated by Zhang [14]. In accordance with the present results, the dual phase lag thermal behavior in tissue should be worthy to have further experimental study. It will be helpful to the relevant developments. The solution of the inverse problem may become sensible to measurement errors of the input data, so this work has no certain values for τ_q and τ_T. The present results can be the reference for further study.

Acknowledgment

Support for this work by the National Science Counsel of the Republic of China under Grant no. 97-2212-E-269-023 is gratefully acknowledged.

Appendix A

1. For direct solution

The Laplace transform technique is used to map the transient problem into the steady one. The differential equations (12) and (13) are transformed under the initial conditions (18) as

$$\frac{d^2\tilde{H}_k}{dr^2} - \lambda_k^2\tilde{H}_k = -f_k r \quad K = 1,2 \tag{A1}$$

where s is the Laplace transform parameter of time t. λ_k^2, f_1, f_2, and K_k are defined as

$$\lambda_k^2 = \frac{1}{K_k}\rho_k c_k s \quad k = 1,2 \tag{A2}$$

$$f_1 = \frac{P(1+\tau_{q1}s)}{k_1(1+\tau_{T1}s)s} \tag{A3a}$$

$$f_2 = 0 \tag{A3b}$$

$$K_k = k_k \frac{1+\tau_{Tk}s}{1+\tau_{qk}s} \quad k = 1,2 \tag{A4}$$

In accordance with Eq. (2), the boundary conditions (14)–(17) in the Laplace transform domain can be written as

$$\tilde{H}_1(0,s) = 0 \tag{A5}$$

$$\tilde{H}_1(R,s) = \tilde{H}_2(R,s) \tag{A6}$$

$$K_1\left(\frac{d\tilde{H}_1(R,s)}{dr} - \frac{\tilde{H}_1}{R}\right) = K_2\left(\frac{d\tilde{H}_2(R,s)}{dr} - \frac{\tilde{H}_2}{R}\right) \tag{A7}$$

$$\tilde{H}_2(\infty,s) = 0 \tag{A8}$$

The present paper divides the whole space domain into several sub-space domains. For continuities of heat flux and temperature within the whole space domain, the following conditions are required at the interface of the sub-space domain j-1, $[r_{i-1}, r_i]$, and the sub-space domain j, $[r_i, r_{i+1}]$.

$$\tilde{H}_{j-1,k}(r_i) = \tilde{H}_{j,k}(r_i) \quad i = 1,2,\ldots,M;\ j = i;k = 1,2 \tag{A9}$$

$$K_k\left(\frac{d\tilde{H}_{j-1,k}(r_i)}{dr} - \frac{\tilde{H}_{j-1,k}}{r_i}\right) = K_k\left(\frac{d\tilde{H}_{j,k}(r_i)}{dr} - \frac{\tilde{H}_{j,k}}{r_i}\right)$$
$$i = 1,2,\ldots,M;j = i;k = 1,2 \tag{A10}$$

where the subscript i is the number of node. M is the total number of nodes.

A modified discretization technique based on Eqs. (A9) and (A10) is developed for the governing algebraic equations in the present work. Before performing the derivation of the governing algebraic equations, $\tilde{H}$ should be approximated by using the nodal temperatures and shape function within a small sub-space domain. The present work derives the shape functions from the governing equation (A1).

For the sub-space domain j, $[r_i, r_{i+1}]$, the analytical solution of the governing equation (A1) subjected to the boundary conditions

$$\tilde{H}_{j,k}(r_i) = \tilde{H}_{i,k} \quad \text{and} \quad \tilde{H}_{j,k}(r_{i+1}) = \tilde{H}_{i+1,k} \tag{A11}$$

are easily obtained and can be written as

$$\tilde{H}_{j,k} = \frac{1}{\sin h\lambda_k}\left\{\left(\tilde{H}_{i,k} - \frac{f_k}{\lambda_k^2}r_i\right)_i \sin h\lambda_k(r_{i+1}-r) + \left(\tilde{H}_{i+1,k} - \frac{f_k}{\lambda_k^2}r_{i+1}\right)\sin h\lambda_k(r-r_i)\right\} + \frac{f_k}{\lambda_k^2}r \tag{A12}$$

Similarly, Eq. (A1) in the sub-space domain j-1, $[r_{i-1}, r_i]$, can be written as

$$\tilde{H}_{j-1,k} = \frac{1}{\sin h\lambda_k}\left\{\left(\tilde{H}_{i-1,k} - \frac{f_k}{\lambda_k^2}r_{i-1}\right)\sin h\lambda_k(r_i-r) + \left(\tilde{H}_{i,k} - \frac{f_k}{\lambda_k^2}r_i\right)\sin h\lambda_k(r-r_{i-1})\right\} + \frac{f_k}{\lambda_k^2}r \tag{A13}$$

where ℓ denotes the length of sub-space domain or the distance between two neighboring nodes. The value of ℓ can be different in the different layer.

Substituting Eqs. (A9), (A12), and (A13) into Eq. (A10) and then evaluating the resulting derivative can lead to the discretized form for the interior nodes in layer k as following

$$\tilde{H}_{i-1,k} - 2\cos h(\lambda_k r)\tilde{H}_{i,k} + \tilde{H}_{i+1,k} = \frac{f_k}{\lambda_k^2}[r_{i-1} - 2r_i\cos h(\lambda_k r) + r_{i+1}] \tag{A14}$$

The discretized form for the node at the interface between layer 1 and layer 2, $r = R$, can be obtained from the boundary condition (A7) and is written as

$$K_1\frac{\lambda_1}{\sin h\lambda_1\ell}\tilde{H}_{i-1,1} - \left(K_1\frac{\lambda_1\cos h\lambda_1\ell}{\sin h\lambda_1\ell} + K_2\frac{\lambda_2\cos h\lambda_2\ell}{\sin h\lambda_2\ell} + \frac{K_2}{R} - \frac{K_1}{R}\right) \times \tilde{H}_{i,(1,2)} + K_2\frac{\lambda_2}{\sin h\lambda_2\ell}\tilde{H}_{i+1,2} = K_1\frac{f_1}{\lambda_1^2}\left[\frac{1}{\sin h\lambda_1\ell}(R-\ell) - \frac{\cos h\lambda_1\ell}{\sin h\lambda_1\ell}R + 1\right] \tag{A15}$$

Eqs. (A14) and (A15) in conjunction with the discretized forms of the boundary conditions can be rearranged as the following matrix equation

$$[B]\{\tilde{H}\} = \{F\} \tag{A16}$$

where $[B]$ is a matrix with complex numbers, $\{\tilde{H}\}$ is a column vector in the Laplace transform domain, and $\{F\}$ is a column vector representing the forcing term. Thereafter, the value of H in the physical domain can be determined with the application of the Gaussian elimination algorithm and the numerical inversion of the Laplace transform [30].

2. For inverse solution

In order to estimate the target parameters from the experimental data, the least-squares minimization technique is applied to minimize the sum of the squares of the deviations between the calculated values and the experimental data at the specified measurement location r_i. The sum of the squares of the deviations between the calculated values and the measurement values can be expressed as

$$E(A_1, A_2, \ldots, A_N) = \sum_{m=1}^{N}\left(\theta_m^{cal} - \theta_m^{mea}\right)^2 \tag{A17}$$

where θ_m^{cal} and θ_m^{mea} are the calculated temperature increase and the measurement temperature increase at the mth time node, respectively. A_n, $n = 1, 2, 3,\ldots, N$, are used to denote the estimated parameters. In this paper, the estimated parameters are the phase lag times, τ_{q0}, τ_{T1}, τ_{q2} and τ_{T2}. The estimated values of A_n are determined with that the value of E is minimum. The computational procedures are described as follows.

First, the initial guesses of A_n are given. Afterwards, the calculated temperature increase θ_m^{cal} at the specified measurement location $r = r_i$ is taken from Eqs. (A14–A16). Deviations between θ_m^{cal} and θ_m^{mea} are expressed as

$$e_m = \theta_m^{cal} - \theta_m^{mea} \quad \text{for } m = 1,2,3,\ldots,N \tag{A18}$$

The next calculated value $\theta_m^{cal,*}$ can be expanded in a first-order Taylor series as

$$\theta_m^{cal,*} = \theta_m^{cal} + \sum_{n=1}^{N}\frac{\partial\theta_m^{cal}}{\partial A_n}dA_n \tag{A19}$$

In order to obtain the derivative $\partial\theta_m^{cal}/\partial A_n$ in Eq. (A19), the next guessed value of A_n, A_n^*, is introduced as

$$A_n^* = A_n + d_n\delta_{mn} \quad \text{for } m,n = 1,2,3,\ldots,N \tag{A20}$$

where d_n denotes the correction. The symbol δ_{mn} is Kronecker delta.

The next calculated value $\theta_m^{cal,*}$, similarly, with respect to A_n^* can be determined from Eqs. (A14–A16). Deviations between $\theta_m^{cal,*}$ and θ_m^{mea} are written as

$$e_m^* = \theta_m^{cal,*} - \theta_m^{mea} \quad \text{for } m = 1,2,3,\ldots,N \tag{A21}$$

The derivative $\partial\theta_m^{cal}/\partial A_n$ can be expressed in the finite-difference form as

$$\omega_{mn} = \frac{\partial\theta_m^{cal}}{\partial A_n} = \frac{\theta_m^{cal,*} - \theta_m^{mea}}{A_n^* - A_n} \quad \text{for } m,n = 1,2,3,\ldots,N \tag{A22}$$

Substituting Eqs. (A18), (A20), and (A21) into Eq. (A22) leads to

$$\omega_{mn} = \frac{e_m^* - e_m}{d_n} \quad \text{for } m,n = 1,2,3,\ldots,N \tag{A23}$$

The Substitution of Eqs. (A22) and (A23) into Eq. (A19) yields

$$\theta_m^{cal,*} = \theta_m^{cal} + \sum_{n=1}^{N}\omega_{mn}d_n^* \quad \text{for } m = 1,2,3,\ldots,N \tag{A24}$$

where $d_n^* = dA_n$ denotes the new correction of A_n.

Substituting Eqs. (A18) and (A21) into Eq. (A24) has

$$e_m^* = e_m + \sum_{n=1}^{N}\omega_{mn}d_n^* \quad \text{for } m = 1,2,3,\ldots,N \tag{A25}$$

In accordance with Eqs. (A17) and (A21), the sum of the squares of the deviations between the calculated values and the measurement values $E(A_1+\Delta A_1, A_2+\Delta A_2,\ldots,A_n+\Delta A_n)$ can be expressed as

$$E = \sum_{m=1}^{N}\left(e_m^*\right)^2 \tag{A26}$$

In order to yield the minimum value of E with respect to A_n, differentiating E corresponding to the new correction d_n^* is performed. Thus the correction equations corresponding to A_n can be expressed as

$$\sum_{l=1}^{N}\sum_{n=1}^{N}\omega_{nl}\omega_{mn}d_l^* = -\sum_{l=1}^{N}\omega_{ml}e_l \quad \text{for } m = 1,2,3,\ldots N \tag{A27}$$

Eq. (A27) is a set of four algebraic equations for the new correction d_n^*. The new correction d_n^* are obtained from Eq. (A26). Hence, the new values of A_n, $A_n + d_n^*$, can be determined.

The above computation procedures were repeated until the value of

$$\left|\frac{\theta_m^{cal} - \theta_m^{mea}}{\theta_m^{mea}}\right| < \varepsilon \quad \text{for } m = 1,2,3,\ldots N \tag{A28}$$

where ε is the standard deviation of the measurements.

Appendix B

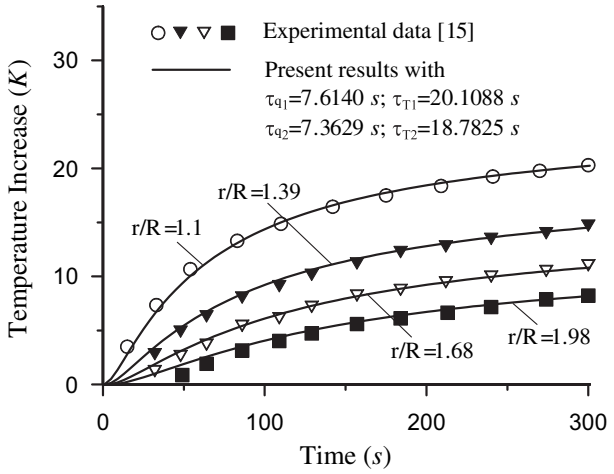

Fig. B1. Variation of temperature increase with the predicted values of τ_{q1}, τ_{T1}, τ_{q2} and τ_{T2} from the measured data at $r/R = 1.39$.

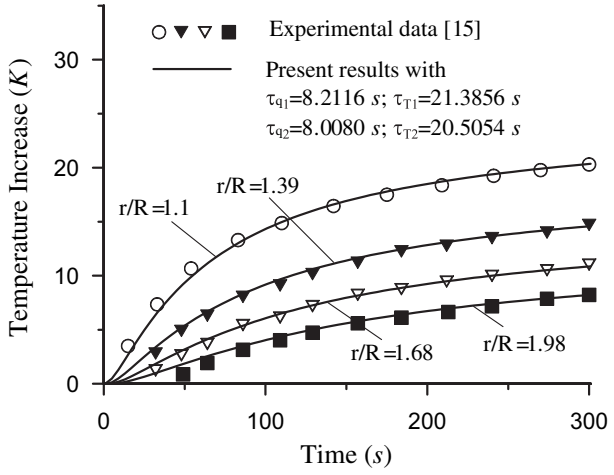

Fig. B2. Variation of temperature increase with the predicted values of τ_{q1}, τ_{T1}, τ_{q2} and τ_{T2} from the measured data at $r/R = 1.68$.

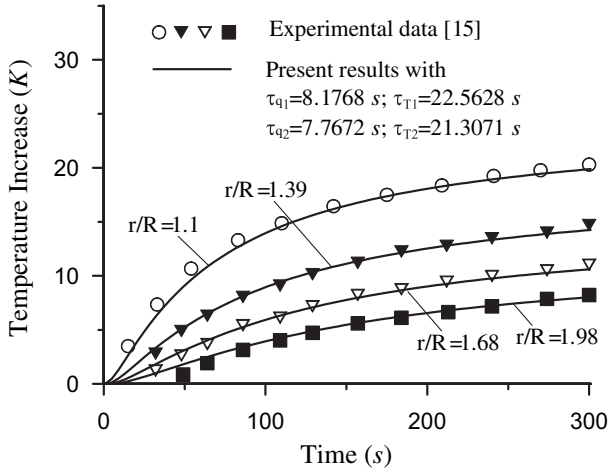

Fig. B3. Variation of temperature increase with the predicted values of τ_{q1}, τ_{T1}, τ_{q2} and τ_{T2} from the measured data at $r/R = 1.98$.

References

[1] L. Zhang, W. Dai, R. Nassar, A numerical method for obtaining an optimal temperature distribution in a 3-D triple-layered cylindrical skin structure embedded with a blood vessel. Numer. Heat Transf. Part A 49 (2006) 765–784.

[2] J. Wren, D. Loyd, M. Karlsson, Investigation of medical thermal treatment using a hybrid bio-heat model, in: Proceedings of the 26th Annual International Conference of the IEEE EMBS San Francisco, CA, USA, September 1–5, 2004.

[3] A.V. Luikov, Analytical Heat Diffusion Theory. Academic Press, New York, 1968.

[4] W. Kaminski, Hyperbolic heat conduction equation for material with a non-homogenous inner structure. ASME J. Heat Transf. 112 (1990) 555–560.

[5] A.M. Braznikov, V.A. Karpychev, A.V. Luikova, One engineering method of calculating heat conduction process. Inzhenerno Fizicheskij Zhurnal 28 (1975) 677–680.

[6] K. Mitra, S. Kumar, A. Vedavarz, M.K. Moallemi, Experimental evidence of hyperbolic heat conduction in processed meat. ASME J. Heat Transf. 117 (1995) 568–573.

[7] W. Roetzel, N. Putra, S.K. Das, Experiment and analysis for non-Fourier conduction in materials with non-homogeneous inner structure. Int. J. Therm. Sci. 42 (2003) 541–552.

[8] W.H. Yang, Thermal (heat) shock biothermomechanical viewpoint. J. Biomed. Eng. 115 (1993) 617–621.

[9] T.C. Shih, H.S. Kou, C.T. Liauh, W.L. Lin, The impact of thermal wave characteristics on thermal dose distribution during thermal therapy: a numerical study. Med. Phys. 32 (2005) 3029–3036.

[10] Ş. Özen, S. Helhel, O. Çerezci, Heat analysis of biological tissue exposed to microwave by using thermal wave model of bio-heat transfer. Burns 34 (2008) 45–49.

[11] K.C. Liu, Thermal propagation analysis for living tissue with surface heating. Int. J. Therm. Sci. 47 (2008) 507–513.

[12] P.J. Antaki, New interpretation of non-Fourier heat conduction in processed meat. ASME J. Heat Transf. 127 (2005) 189–193.

[13] K.C. Liu, H.T. Chen, Analysis for the dual-phase-lag bio-heat transfer during magnetic hyperthermia treatment. Int. J. Heat Mass Transf. 52 (2009) 1187–1192.

[14] Y. Zhang, Generalized dual-phase-lag bioheat equations based on non-equilibrium heat transfer in living biological tissues. Int. J. Heat Mass Transf. 52 (2009) 4829–4834.

[15] W. Andrä, C.G. d'Ambly, R. Hergt, I. Hilger, W.A. Kaiser, Temperature distribution as function of time around a small spherical heat source of local magnetic hyperthermia. J. Magn. Magn. Mater. 194 (1999) 197–203.

[16] H.T. Chen, S.Y. Peng, P.C. Yang, L.C. Fang, Numerical method for hyperbolic inverse heat conduction problems. Int. Commun. Heat Mass Transf. 28 (6) (2001) 847–856.

[17] C.Y. Yang, Direct and inverse solutions of hyperbolic heat conduction problems. J. Thermophys. Heat Transf. 19 (2005) 217–225.

[18] C.Y. Yang, Estimation of the period thermal conditions on the non-Fourier fin problem. Int. J. Heat Mass Transf. 48 (2005) 3506–3515.

[19] C.H. Huang, H.H. Wu, An inverse hyperbolic heat conduction problem in estimating surface heat flux by conjugate gradient method. J. Phys. D: Appl. Phys. 39 (2006) 4087–4096.

[20] C.H. Huang, C.Y. Lin, Inverse hyperbolic conduction problem in estimating two unknown surface heat fluxes simultaneously. J. Thermophys. Heat Transf. 22 (2008) 766–774.

[21] K.C. Liu, Simultaneous estimation of relaxation time and diffusion coefficient during the rapid transient mass transfer. J. Chin. Soc. Mech. Eng. 28 (2007) 541–548.

[22] H.G. Bagaria, D.T. Johnson, Transient solution to the bioheat equation and optimization for magnetic fluid hyperthermia treatment. Int. J. Hyperthermia 21 (2005) 57–75.

[23] S. Maenosono, S. Saita, Theoretical assessment of FePt nanoparticles as heating elements for magnetic hyperthermia. IEEE Trans. Magn. 42 (2006) 1638–1642.

[24] Z.P. Chen, R.B. Roemer, The effects of large blood vessels on temperature distributions during simulated hyperthermia. ASME J. Biomech. Eng. 114 (1992) 473–481.

[25] D.Y. Tzou, Macro- to Microscale Heat Transfer – The Lagging Behavior. Taylor & Francis, Bristol, PA, 1996.

[26] M.N. Özisik, Heat Conduction. John Wiley and Sons, New York, 1993.

[27] K.C. Liu, Analysis of dual-phase-lag thermal behavior in layered films with temperature-dependent interface thermal resistance. J. Phys. D: Appl. Phys. 38 (2005) 3722–3732.

[28] K.C. Liu, P.J. Cheng, Numerical analysis for dual-phase-lag heat conduction in layered films. Numer. Heat Transf. Part A 49 (2006) 589–606.

[29] K.C. Liu, Numerical analysis of dual-phase-lag heat transfer in a layered cylinder with nonlinear interface boundary conditions. Comput. Phys. Commun. 177 (2007) 307–314.

[30] G. Honig, U. Hirdes, A method for the numerical inversion of Laplace transforms. J. Comput. Appl. Math. 10 (1984) 113–132.